Korean J. Chem. Eng., 37(12), 2326-2333 (2020)
DOI: 10.1007/s11814-020-0669-0

pISSN: 0256-1115
eISSN: 1975-7220

The effects of temperature and membrane thickness on the performance of aqueous alkaline redox flow batteries using napthoquinone and ferrocyanide as redox couple

Wonmi Lee*, Gyunho Park*, Dukrye Chang,†, and Yongchai Kwon*,***,†**

*Graduate School of Energy and Environment, Seoul National University of Science and Technology, 232 Gongneung-ro, Nowon-gu, Seoul 01811, Korea
**Gwangju Research Center, Korea Institute of Industrial Technology, Gwangju 61012, Korea
***Department of Chemical and Biomolecular Engineering, Seoul National University of Science and Technology, 232 Gongneung-ro, Nowon-gu, Seoul 01811, Korea
(*Received 9 April 2020 • Revised 23 June 2020 • Accepted 27 August 2020*)

Abstract−The mixture of naphthoquinone-4-sulfonic acid sodium salt and 2-hydroxy-naphthoquinone (NQSO) and ferrocyanide dissolved in potassium hydroxide (KOH) electrolyte was used as catholyte and anolyte, respectively. We evaluated the effects of temperature and membrane thickness on the performance of aqueous organic redox flow batteries (AORFB) using the NQSO and ferrocyanide dissolved in alkaline electrolyte. Regarding temperature effect, when the electrochemical properties of NQSO and ferrocyanide are evaluated with 25 and 40 °C, their redox reactivity is enhanced with increased temperature due to the proportional relation of reaction rate and temperature. In addition, their electron transfer rate is also improved with increased temperature due to the proportional relation of electron transfer rate and temperature. These are proven by Nyquist plots showing the reciprocal relationship of resistance and temperature. In AORFB full cell tests performed at 25 and 40 °C, although capacity decay rate observed at 40 °C (0.067 $Ah \cdot L^{-1}$ per cycle) is larger than that observed at 25 °C (0.034 $Ah \cdot L^{-1}$ per cycle), energy efficiency (EE) was improved from 86% at 25 °C to 89% at 40 °C. Regarding membrane thickness effect, the performance of AORFB using thin Nafion 212 membrane is better than that of AORFBs using thick Nafion 117 and Nafion 1110 membranes in voltage efficiency (VE) and EE, while its capacity retention is vice versa. This is because thinner membrane induces lower resistance.

Keywords: Naphthoquinone-4-sulfonic Acid Sodium Salt and 2-Hydroxy-naphthoquinone, Ferrocyanide, Aqueous Organic Redox Flow Battery, Temperature Effect, Membrane Thickness Effect

INTRODUCTION

Energy storage systems (ESS) have to be developed to use renewable energy effectively [1-20]. As ESS candidates, there are hydropower, flywheels, batteries and fuel cells [1-15]. Among them, lithium-ion batteries have been widely used for commercial applications due to their high energy density [16-20]. However, their easy flammability and the flammability related accidents must be overcome [21,22].

As an alternative to solve this easy flammability issue, redox flow battery (RFB) can be considered [23-30]. RFB has various advantages. For example, the energy and power can be separately produced by controlling the tank and electrode size [23]. This RFB consists of two electrolytes containing active materials, two electrodes where redox reactions take place, membrane which prevents the cross-over of active materials and transfers the charge carries, current collectors, and bipolar plates [24]. The active materials that are dissolved in supporting electrolyte should have excellent electrochemical property, such as a high solubility and a wide cell voltage [25]. Regarding electrodes, they should promote electron transfer. To meet the need, carbon materials, such as carbon felt or carbon paper, have been used [26,27]. Likewise, membranes should have a high selectivity, which means that the cross-over of active materials has to be suppressed, while the charge carriers, such as protons or hydroxide ions, have to be transferred well through the membrane over the long cycle with a high energy efficiency (EE) [28-30].

Active materials for RFB have been usually metal ions due to a high solubility and good redox properties, such as reactivity, electron transfer rate, and reversibility [31-54]. For example, iron-chromium RFB (Fe-Cr RFB), zinc-bromine RFB (Zn-Br RFB), and vanadium RFB (VRFB) have been developed [35-43]. Among them, VRFB has been mostly developed in research area and used as commercial system all over the world due to various benefits. First is relatively longer cycle stability than the other metal-based RFBs because the active materials, vanadium ions, are used in both electrolytes [35,36]. They have four oxidation states (V^{2+}, V^{3+}, V^{4+}, and V^{5+}), and therefore, they are used as active material for both positive and negative electrode, which leads to a low cross-over by the utilization of the same active material [37-42]. Second is their high solubility in sulfuric acid, which leads to a high ionic conductivity and EE [43]. However, RFB has still some hurdles to overcome for use in commercial applications [44-51]. First, vanadium is expensive because it is a rare metal [44]. Second, the membrane is also expensive, so the overall system cost is high [45]. Third, the operational temperature range is narrow because the precipitation of vanadium ions occurs under 0 °C or upper 45 °C [46]. Fourth,

†To whom correspondence should be addressed.
E-mail: drchang@kitech.re.kr, kwony@seoultech.ac.kr

expensive catalyst is usually required to enhance the redox reactivity of vanadium ions, especially that for V^{4+}/V^{5+} redox reaction [47-54].

To solve these problems, organic materials have been introduced as active material instead of vanadium. They are produced in a large quantity at low cost, while their redox reactivity and solubility can be tuned by adopting proper functional groups [55-63]. Such organic material based RFBs can be categorized by the type of supporting electrolyte as non-aqueous RFB and aqueous RFB [58-74]. There are pros and cons for each type of RFB. Non-aqueous RFB has the benefit of unlimited operating voltage range because water electrolysis does not occur [58,59]. However, this is easily flammable, and thus, dangerous accidents may occur [60,61]. In contrast, aqueous RFB is safe about the flammability issue, while its ionic conductivity is higher than that of non-aqueous RFB, leading to a high power density.

To alleviate the above issues, aqueous organic redox flow batteries (AORFBs) are suggested [64-74], and there have been already some research results. For example, the Aziz group introduced 9,10-anthraquinone-2,7-disulphonic acid (AQDS) as negative side active material and bromide as positive side active material [64]. Narayanan group used quinones in both sides as active materials for all-quinone redox flow batteries. More specifically, 4,5-Dihydroxy-1,3-benzenedisulfonic acid (BQDS) was used as active material for positive side and 9,10-anthraquinone-2,6-disulphonic acid (AQDS) was used as active material for negative side in sulfuric acid electrolyte [65].

One step further, to increase cell voltage, alkaline electrolyte was used to modulate the redox potential of active material belonging to negative electrode [66-70]. For example, the Aziz group developed 2,6-dihydroxyanthraquinone (2,6-DHAQ) and ferrocyanide as negative and positive active materials in KOH, respectively. The open circuit voltage (OCV) of AORFB using the redox couple increased to 1.2 V, which led to a high power density (0.7 $W \cdot cm^{-2}$) [67]. The chemical stability of anthraquinone derivative was also enhanced by the use of this redox couple, and such enhanced chemical stability induced the enhancement in cycle stability [69].

However, the above approaches were performed under the condition of room temperature and a single membrane was used. This means that there have been few researches on the effects of temperature and membrane thickness on the performance and stabil-

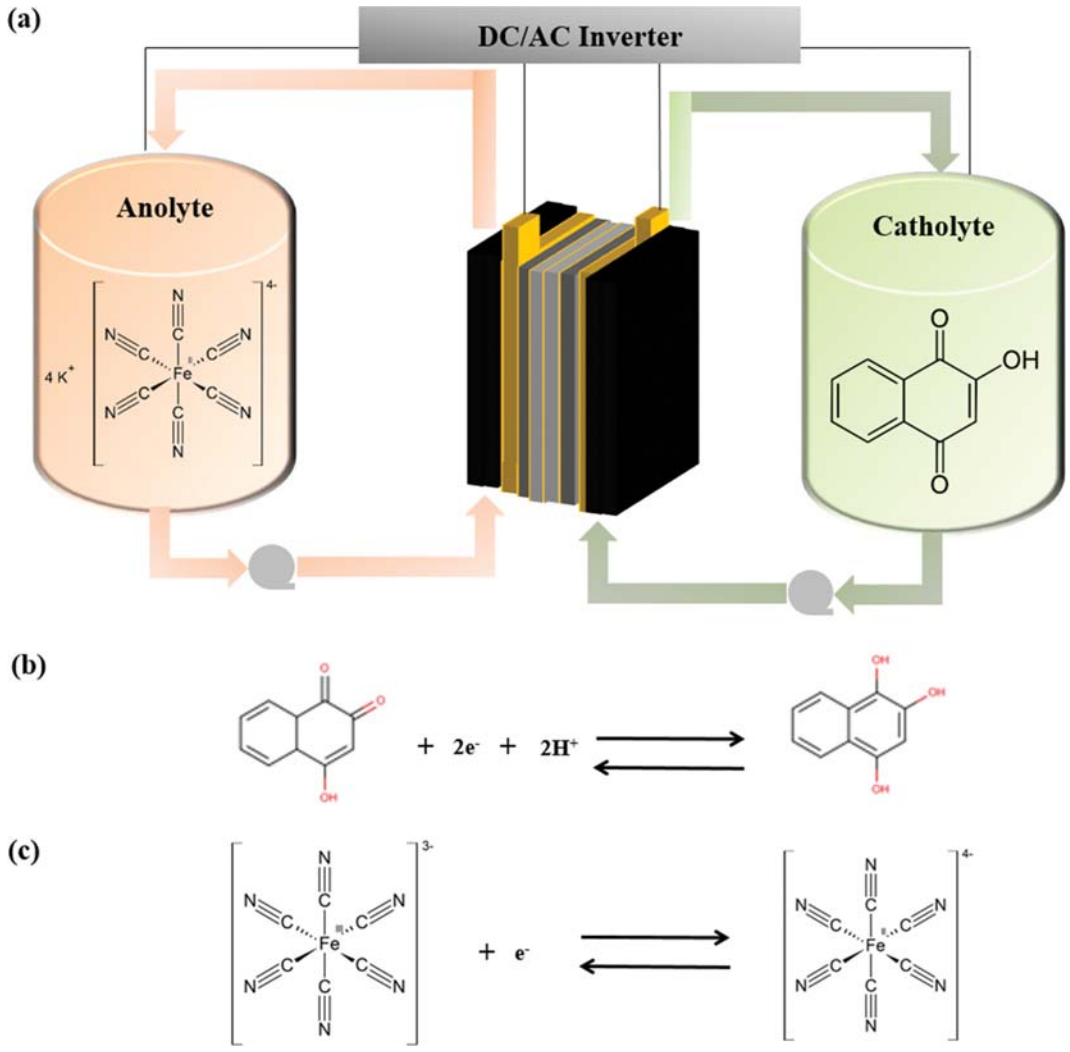

Fig. 1. Schematic of (a) AORFB full cell structure and the redox reactions of (b) NQSO and (c) ferrocyanide.

ity of AORFBs.

Due to the above demands, in this study, we investigated the effects of temperature and membrane thickness on the performance and stability of AORFBs using the mixture of naphthoquinone-4-sulfornic acid sodium salt and 2-hydroxy-naphthoquinone (NQSO) and ferrocyanide as redox couple, which is dissolved in KOH. Although the performance of AORFB using NQSO and ferrocyanide redox couple was already reported by our group, how the temperature and membrane thickness affect the performance and stability of AORFBs has not been studied yet. The design of the AORFB full cell and the redox reactions of active materials are shown in Fig. 1.

EXPERIMENTAL

1. Materials

To prepare a catholyte and anolyte consisting of NQSO and ferrocyanide, naphthoquinone-4-sulfonic acid sodium salt and 2-hydroxy naphthoquinone were purchased from Alfa Aesar. Potassium hexacyanoferrate(II) trihydrate was bought from Sigma Aldrich. Potassium hydroxide (95.0%) that was used for supporting electrolyte solution was obtained from Samchun Chemical. In addition, various types of Nafion membranes (Nafion 212 (N212), Nafion 117 (N117), and Nafion 1110 (N1110)) were bought from the Sigma Aldrich and put in de-ionized (DI) water for 24 h before use.

2. Electrochemical Measurements

2-1. Electrochemical Characterizations

To investigate the effect of temperature on the electrochemical properties of NQSO and ferrocyanide, their cyclic voltammogram (CV) curves and Nyquist plots using electrochemical impedance spectroscopy (EIS) were measured at different temperatures (25 and 40 °C). Pt wire and Ag/AgCl were used as counter and reference electrodes, respectively, and glass carbon electrode (GCE, 5 mm diameter, active area 0.196 cm^2) was considered as working electrode. The scan rate used was 100 $mV \cdot s^{-1}$. As electrolytes, 0.01 M of both NQSO and ferrocyanide was dissolved into 20 mL of 1.0 M KOH solution.

Furthermore, the samples of before and after AORFB full cell test were collected and their CV curves were measured to investigate how the cross-over of active materials through membrane was affected by temperature. To evaluate the relationship between membrane thickness and the resistance of electrolyte, Nyquist plots of Nafion membranes with three different thicknesses (N212, N117, and N1110) were measured.

2-2. The Performance Evaluations of AORFB Full Cells

For AORFB full cell tests, charge-discharge equipment (Wonatech, WBCS3000) was used. As catholyte, 0.3 M of NQSO was dissolved in 1.0 M KOH solution and 20 mL of the prepared catholyte was filled with tank, while 0.3 M of ferrocyanide was dissolved in 1.0 M KOH solution as anolyte and 50 mL of the prepared catholyte filled the tank. An excessive amount of ferrocyanide was used to fix the redox reaction of anolyte as a rate determining step. Carbon felt (SGL 4.6 GFD, active area of 6 cm^2 and thickness of 4.7 mm) was used as electrode. During charge and discharge cycle, 40 $mA \cdot cm^{-2}$ was applied under the cut-off voltage ranges of 0.2-1.6 V.

To investigate the temperature effect on the performance of

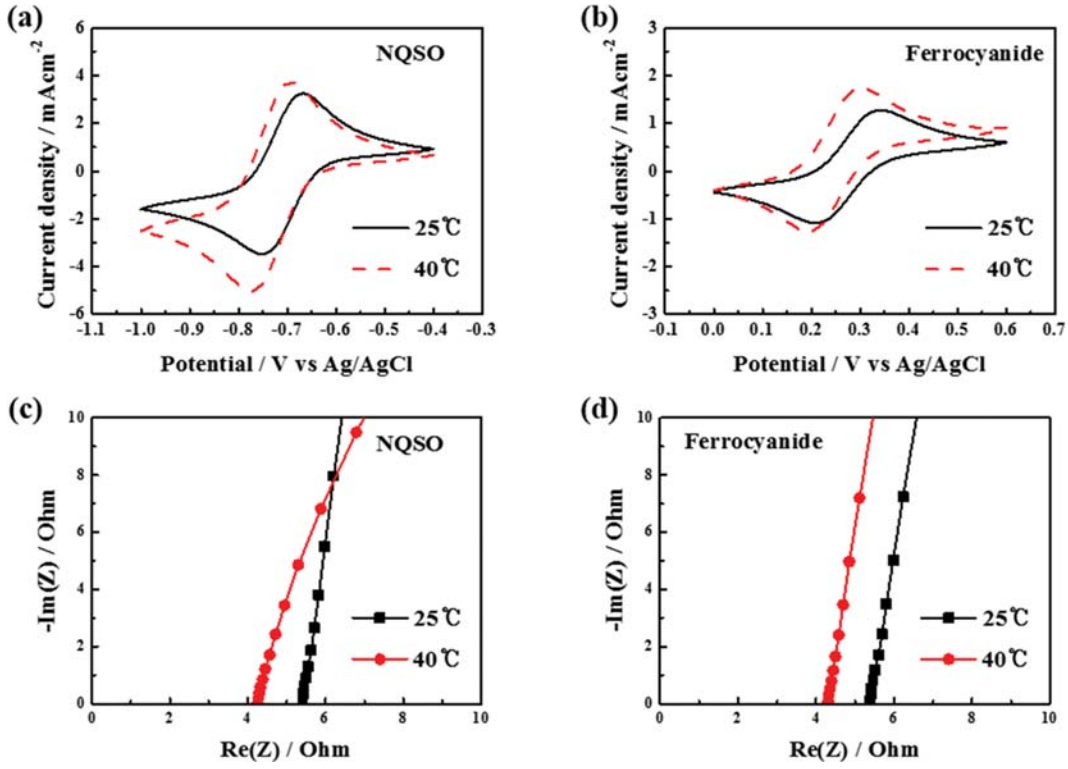

Fig. 2. CV curves representing the redox reactivity of (a) NQSO and (b) ferrocyanide measured at different temperatures (25 and 40 °C) with a scan rate of 100 mV s^{-1} and Nyquist plots of (c) NQSO and (d) ferrocyanide dissolved 1.0 M KOH at different temperatures (25 and 40 °C).

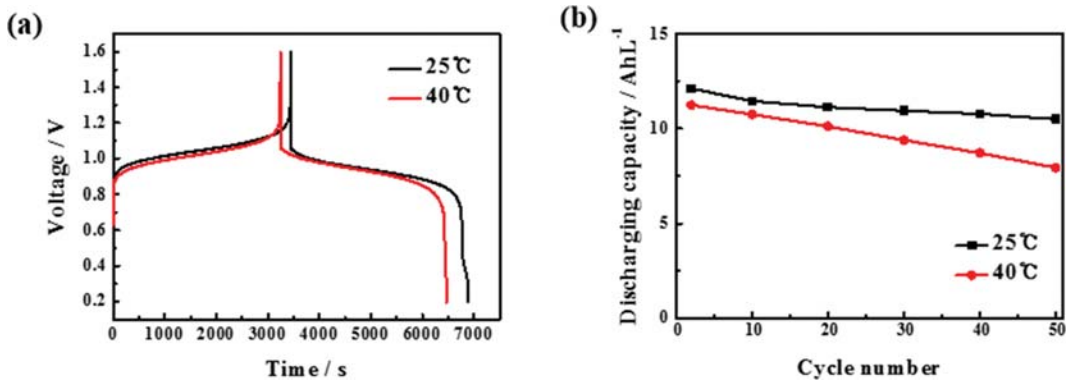

Fig. 3. (a) Charge-discharge curves of AORFBs using NQSO and ferrocyanide as redox couple measured at 10th cycle and (b) their discharging capacities measured at different temperatures (25 and 40 °C).

AORFB using NQSO and ferrocyanide, two temperatures of 25 and 40 °C were selected with the use of Nafion 212 membrane. To evaluate the effect of membrane thickness on the performance of AORFB, three different Nafion membranes (N212, N117, and N1110) were used and all the AORFB full cell tests were operated at 40 °C. In addition, all membranes were pre-treated in DI water for 24 h before use.

RESULTS AND DISCUSSION

1. The Effect of Temperature on the Electrochemical Properties of NQSO and Ferrocyanide

To evaluate the effect of temperature on the electrochemical properties of NQSO and ferrocyanide, CV curves and Nyquist plots of the active materials dissolved in KOH were measured in 25 and 40 °C (Fig. 2). According to the CV curves of Figs. 2(a) and (b), the redox reactivity and electron transfer rates of both NQSO and ferrocyanide were enhanced at 40 °C. More specifically, in terms of the redox reactivity of NQSO, the oxidation current peak was improved from 3.2 $mA \cdot cm^{-2}$ at 25 °C to 3.7 $mA \cdot cm^{-2}$ at 40 °C, and the reduction current peak was improved from −3.5 $mA \cdot cm^{-2}$ to −5.1 $mA \cdot cm^{-2}$. Likewise, in ferrocyanide, its oxidation current peak was increased from 1.3 $mA \cdot cm^{-2}$ at 25 °C to 1.7 $mA \cdot cm^{-2}$ at 40 °C and the reduction current peak was improved from −1.1 $mA \cdot cm^{-2}$ to −1.3 $mA \cdot cm^{-2}$ 40 °C. This means that the redox reaction of both NQSO and ferrocyanide became faster with an increase in temperature due to Arrhenius' equation that shows the relationship between reaction rate constant and temperature [75]. Namely, as the temperature increases, the reaction rate constant and redox reactivity are improved.

Meanwhile, in terms of the electron transfer rate, as the peak separation between oxidation and reduction potentials was reduced, the electron transfer rate became faster. The redox potential peak separation of NQSO was reduced from 0.09 V at 25 °C to 0.08 V at 40 °C. The value of ferrocyanide was also decreased from 0.14 to 0.11 V. This also indicates that the electron transfer rate was enhanced with an increase in temperature due to Marcus theory that shows the relationship between electron transfer rate constant and temperature [76]. Namely, as the temperature increased, the electron transfer rate constant also increased, and this led to the faster electron transfer.

The above result was confirmed by measuring the Nyquist plots using EIS of NQSO and ferrocyanide in 25 and 40 °C (Figs. 2(c) and (d)). The resistance of NQSO was reduced from 5.4 Ω at 25 °C to 4.3 Ω at 40 °C. Likewise, the resistance of ferrocyanide was decreased from 5.4 to 4.3 Ω Since the resistance measured by Nyquist plot is related to electron transfer rate, a low resistance induces a fast electron transfer rate [77].

Next, to evaluate the effect of temperature on the performance of AORFB using NQSO and ferrocyanide dissolved in 1.0 M KOH, its charge-discharge curves were measured at 25 and 40 °C (Fig, 3). Nafion 212 membrane was used as separator to prevent the cross-over of active materials and to transfer the potassium ions well through the membrane [78]. According to Fig. 3(a), as temperature increased, the pattern of charge and discharge curves was similar, while over-potential was reduced. This is due to the decrease in resistance evaluated at a higher temperature, and this fact well matched the results in CV and EIS (Fig. 2). In terms of capacity, when the discharging capacity measured in different temperatures was compared (Fig. 3(b)), although this was similar for the first few cycles, as the cycle number increased, the value measured at 25 °C was better than that measured at 40 °C. More specifically, the discharging capacity was well preserved from the initial capacity (12.1 $Ah \cdot L^{-1}$) to the capacity after 50 cycles (10.4 $Ah \cdot L^{-1}$) with a high capacity retention rate (0.034 $Ah \cdot L^{-1}$ loss rate per cycle) at 25 °C. However, when the temperature increased to 40 °C, the capacity retention rate (0.067 $Ah \cdot L^{-1}$ loss rate per cycle) was reduced due to a higher capacity loss from the initial capacity (11.2 $Ah \cdot L^{-1}$) to the capacity after 50 cycles (7.9 $Ah \cdot L^{-1}$). This can be explained as when the temperature increases, the cross-over of active materials through the membrane also increases because their diffusion rate is proportional to temperature [79]. Eventually, as temperature increased, capacity retention rate was reduced.

In terms of the efficiencies, the comparison result of AORFBs measured at 25 and 40 °C is represented in Fig. 4. Differently from the initial guess that columbic efficiency (CE) would be decreased with increasing temperature, CE of both AORFBs maintained 99% of its initial value during cycling. This CE result, which was independent of temperature, is because the active materials have a higher selectivity regarding the permeability of ions through the

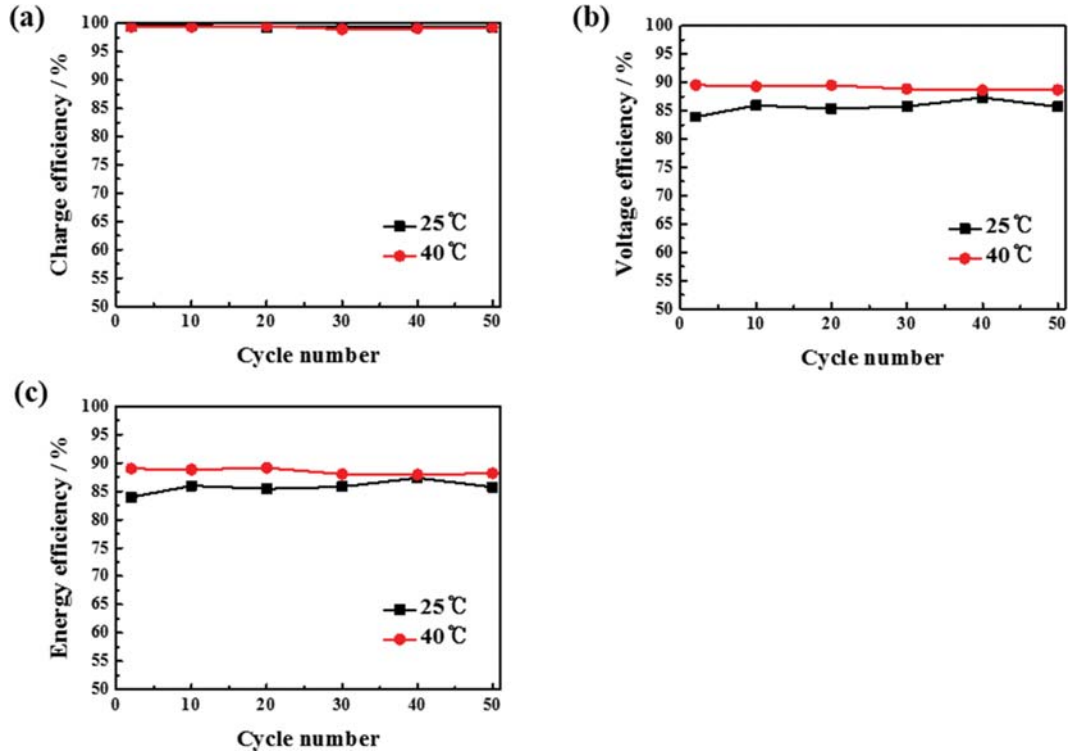

Fig. 4. (a) Columbic efficiency, (b) voltage efficiency and (c) energy efficiency graphs measured during cycling of AORFBs using NQSO and ferrocyanide in different temperatures (25 and 45 °C).

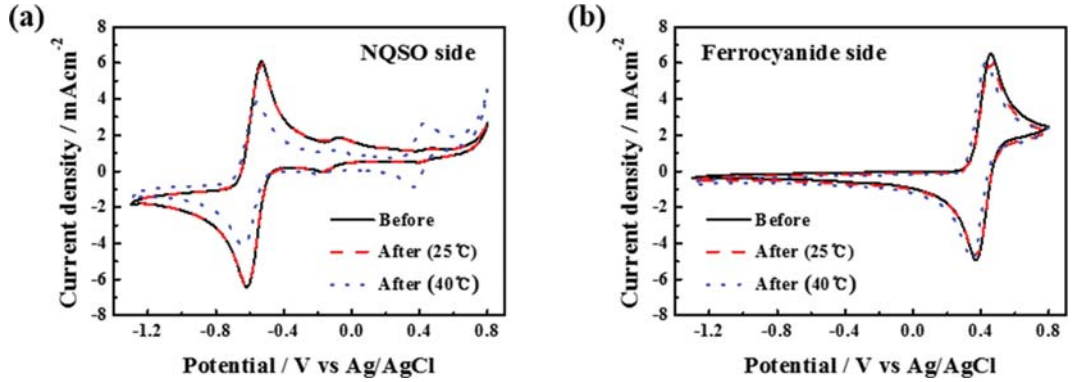

Fig. 5. CV curves of (a) NQSO and (b) ferrocyanide solutions before and after AORFB tests measured at different temperatures (25 and 45 °C).

membrane. On the other hand, the voltage efficiency (VE) was enhanced from 86% (at 25 °C) to 89% (at 40 °C). This is because VE is affected by the charge transfer rate of active materials that is proportional to temperature [80]. This VE pattern is compatible with the trend of CV curve data (Figs. 2(a) and 2(b)). Namely, as temperature increased, the charge transfer resistance was reduced, which then promoted the decrease in over-potential and increase in VE during the cycling [80]. Based on the CE and VE, the energy efficiency (EE) was increased from 86% (at 25 °C) to 89% (at 40 °C).

To identify the effect of temperature on the cross-over of active materials through the membrane, CV curves of samples collected before and after AORFB full cell tests performed in different temperatures were measured (Fig. 5). In case of 25 °C, the cross-over of both NQSO and ferrocyanide was not observed. However, in 40 °C, the cross-over of ferrocyanide was observed. This demonstrates that as temperature increases, the cross-over of ferrocyanide is facilitated due to its increased diffusion rates, and the high cross-over of ferrocyanide is probably due to molecule size, meaning that that of ferrocyanide (radius of 5.8 Å) is smaller than that of NQSO (radius of 7.6 Å) [81,82].

2. The Effect of Membrane Thickness on the Performance of AORFBs using NQSO and Ferrocyanide

To identify the effect of membrane thickness on the performance of AORFBs using NQSO and ferrocyanide as redox couple, AORFB full cell tests including three different Nafion membranes (N212 (thickness 50.8 μm), N117 (thickness 183 μm), N1110 (thickness

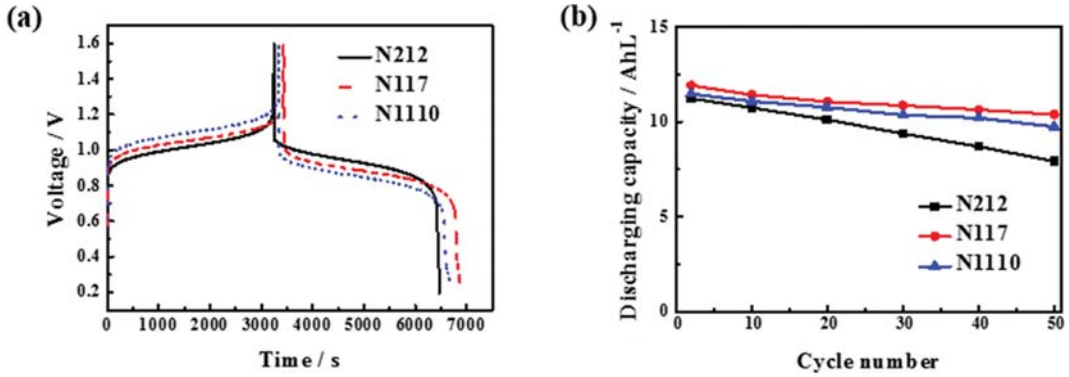

Fig. 6. (a) Charge-discharge curves of AORFBs using NQSO and ferrocyanide as redox couple measured at 10th cycle and (b) their discharging capacities measured in different Nafion membranes (N212, N117 and N1110).

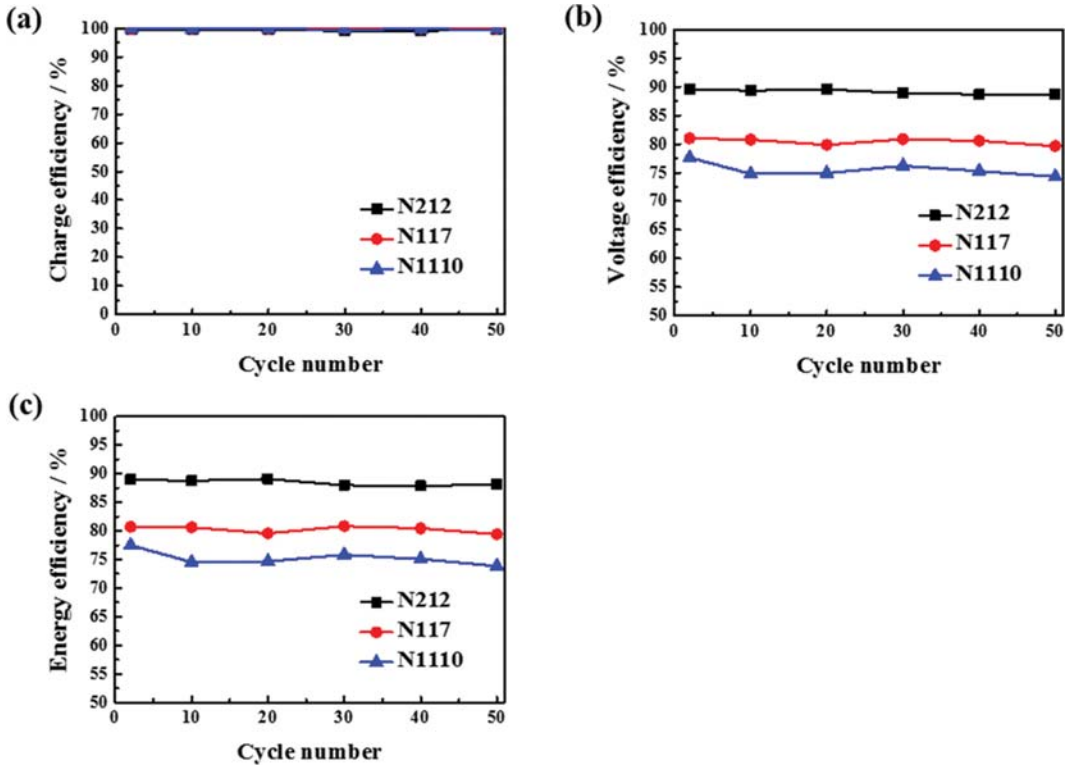

Fig. 7. (a) Columbic efficiency, (b) voltage efficiency and (c) energy efficiency graphs measured during cycling of AORFBs using NQSO and ferrocyanide in different Nafion membranes (N212, N117 and N1110).

254 μm)) were implemented. The other operational conditions were the same with the operational temperature of 40 °C. Their charge-discharge curves and discharging capacity pattern are shown in Fig. 6. As shown in Fig. 6(a), the pattern of charge-discharge curves was very similar in AORFBs using all Nafion membranes. This is due to the same properties of Nafion membranes except thickness. Differently from that, the different factor to be affected by different thicknesses is over-potential. When the thickness of membrane increases, the over-potential usually increases. In contrast, in terms of capacity retention, thicker membrane induces a better capacity retention. This is because the thicker membrane can mitigate the cross-over of active materials which leads to higher capacity retention (Fig. 6(b)). More specifically, in AORFB using the thinnest membrane (N212), the initial discharging capacity was 11.2 $Ah \cdot L^{-1}$ and it was reduced to 7.9 $Ah \cdot L^{-1}$ after 50 cycles with the lowest capacity retention (loss rate per cycle of 0.067 $Ah \cdot L^{-1}$). On the other hand, in AORFBs the thicker membranes (N117 and N1110) than N212, the initial discharging capacities were 11.9 and 11.4 $Ah \cdot L^{-1}$ and those were decreased to 10.3 and 9.7 $Ah \cdot L^{-1}$, respectively. The capacity retention rate of AORFBs using N117 and N1110 was similar (0.032 $Ah \cdot L^{-1}$ (N117) and 0.034 (N1110) $Ah \cdot L^{-1}$ per cycle). It means that as the membrane becomes thicker, its capacity is well preserved during cycling. Based on that, N117 is the reasonable thickness for the stable cycling of AORFB because its capacity retention was similar to AORFB using N1110, while its VE and EE were higher than AORFB using N1110.

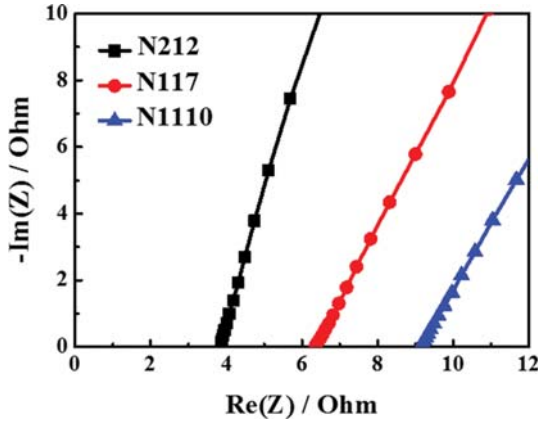

Fig. 8. Nyquist plots of three Nafion membranes with different thicknesses dissolved in 1.0 M KOH solution.

The effect of membrane thickness on the efficiency of AORFBs using NQSO and ferrocyanide is represented in Fig. 7. According to Fig. 7, CE of the three AORFBs using different Nafion membranes was almost same as 99% during cycling. As explained earlier, this is because the active materials have a high selectivity through the membrane due to its relatively larger molecular size than metal ions such as vanadium. Differently from CE, VE was significantly affected by the thickness of membrane. The VEs of AORFBs using N212, N117, and N1110 were 89, 80, and 75%, respectively. Thus, as the thickness of membrane increased, VE was reduced. This result is due to the relationship between conductivity and membrane thickness [83]. The conductivity depends on membrane thickness, membrane resistance, and the area of electrodes. Here, the area of electrode is the same. Thus, the conductivity relies on the membrane resistance in different membrane thickness. To identify the relationship between conductivity and Nafion membrane thickness, their Nyquist plots using EIS were performed (Fig. 8). According to Fig. 8, the resistance of N212, N117 and N1110 was 3.86, 6.35 and 9.17 Ω Under the similar CE condition, since VE handles EE, the EE of AORFBs using N212, N117 and N1110 was 89, 80, and 75%.

CONCLUSION

The effects of temperature and membrane thickness on the performance of alkaline pH AORFB using NQSO and ferrocyanide were investigated. In terms of the redox reactivity of NQSO and ferrocyanide, as temperature increased, electron transfer rate and redox reactivity were improved. Based on the electrochemical evaluations of redox couple, when the AORFB full cell tests were performed, as temperature increased their VE and EE were enhanced, whereas capacity retention rate was reduced. This opposite pattern of efficiencies and capacity retention is because as temperature increases, the diffusion rate of the active materials is faster and the crossover through the membranes is severer.

In addition, the membrane thickness was also an important factor to affect the performance of AORFBs because the resistance was highly related to the membrane thickness. The thinner membrane induced a lower resistance, leading to a higher VE. Therefore, VE and EE were improved in AORFB using thinner membrane. However, the capacity retention rate was decreased. Taken together, by the optimization of temperature and membrane thickness during cycling of AORFBs, the efficiency and capacity retention could be improved and optimized for improving the performance of AORFB.

ACKNOWLEDGEMENT

This study was supported by the Research Program funded by the SeoulTech (Seoul National University of Science and Technology).

REFERENCES

1. L. E. Benitez, P. C. Benitez and G. C. Van Kooten, *Energy Econ.*, **30**, 1973 (2008).
2. M. E. Amiryar and K. R. Pullen, *Appl. Sci.*, **7**, 286 (2017).
3. M. Bortolini, M. Gamberi and A. Graziani, *Energy Convers. Manag.*, **86**, 81 (2014).
4. X. Hu, L. Johannesson, N. Murgovski and B. Egardt, *Appl. Energy*, **137**, 913 (2015).
5. R. T. Doucette and M. D. McCulloch, *J. Power Sources*, **196**, 1163 (2011).
6. J. E. Lim and J. K. Kim, *Korean J. Chem. Eng.*, **35**, 2464 (2018).
7. R. Andika, Y. Kim, C. M. Yun, S. H. Yoon and M. Lee, *Korean J. Chem. Eng.*, **36**, 12 (2019).
8. S. Lee, B. Gendensuren, B. Kim, S. Jeon, Y. H. Cho, T. Kim and E. S. Oh, *Korean J. Chem. Eng.*, **36**, 1940 (2019).
9. J. H. Kim, S. A. Jun, Y. Kwon, S. Ha, B. I. Sang and J. Kim, *Bioelectrochemistry*, **101**, 114 (2015).
10. K. Hyun, S. W. Han, W. G. Koh and Y. Kwon, *Int. J. Hydrogen Energy*, **40**, 2199 (2015).
11. K. H. Hyun, S. W. Han, W. G. Koh and Y. Kwon, *J. Power Sources*, **286**, 197 (2015).
12. M. Christwardana and Y. Kwon, *J. Power Sources*, **299**, 604 (2015).
13. Y. Chung, K. H. Hyun and Y. Kwon, *Nanoscale*, **8**, 1161 (2016).
14. Y. Chung, Y. Ahn, M. Christwardana, H. Kim and Y. Kwon, *Nanoscale*, **8**, 9201 (2016).
15. M. Christwardana, K. J. Kim and Y. Kwon, *Sci. Rep.*, **6**, 1 (2016).
16. N. Mahmood, C. Zhang, H. Yin and Y. Hou, *J. Mater. Chem. A*, **2**, 15 (2014).
17. M. M. Thackeray, C. Wolverton and E. D. Isaacs, *Energy Environ. Sci.*, **5**, 7854 (2012).
18. C. Sun, J. Liu, Y. Gong, D. P. Wilkinson and J. Zhang, *Nano Energy*, **33**, 363 (2017).
19. H. S. Ko, H. W. Park, G. J. Kim and J. D. Lee, *Korean J. Chem. Eng.*, **36**, 620 (2019).
20. W. G. Lim, C. Jo, J. Lee and D. S. Hwang, *Korean J. Chem. Eng.*, **35**, 579 (2018).
21. J. Hassoun, S. Panero, P. Reale and B. Scrosati, *Adv. Mater.*, **21**, 4807 (2009).
22. M. Masih-Tehrani, M. R. Ha'iri-Yazdi, V. Esfahanian and A. Safaei, *J. Power Sources*, **244**, 2 (2013).
23. P. Leung, X. Li, C. P. De León, L. Berlouis, C. J. Low and F. C. Walsh, *Rsc Adv.*, **2**, 10125 (2012).
24. J. Winsberg, T. Hagemann, T. Janoschka, M. D. Hager and U. S. Schubert, *Angew. Chem. Int. Ed.*, **56**, 686 (2017).

25. M. Bartolozzi, *J. Power Sources*, **27**, 219 (1989).
26. B. R. Chalamala, T. Soundappan, G. R. Fisher, M. R. Anstey, V. V. Viswanathan and M. L. Perry, *Proc. IEEE*, **102**, 976 (2014).
27. T. Sasaki, T. Kadoya and K. Enomoto, *IEEE Trans. Power Syst.*, **19**, 660 (2004).
28. F. Pan and Q. Wang, *Molecules*, **20**, 20499 (2015).
29. X. L. Zhou, T. S. Zhao, L. An, Y. K. Zeng and L. Wei, *J. Power Sources*, **339**, 1 (2017).
30. M. H. Chakrabarti, F. S. Mjalli, I. M. AlNashef, M. A. Hashim, M. A. Hussain, L. Bahadori and C. T. J. Low, *Renew. Sustain. Energy Rev.*, **30**, 254 (2014).
31. W. Lee, B. W. Kwon, M. Jung, D. Serhiichuk, D. Henkensmeier and Y. Kwon, *J. Power Sources*, **439**, 227079 (2019).
32. M. Lopez-Atalaya, G. Codina, J. R. Perez, J. L. Vazquez and A. Aldaz, *J. Power Sources*, **39**, 147 (1992).
33. J. D. Jeon, H. S. Yang, J. Shim, H. S. Kim and J. H. Yang, *Electrochim. Acta*, **127**, 397 (2014).
34. J. H. Yang, H. S. Yang, H. W. Ra, J. Shim and J. D. Jeon, *J. Power Sources*, **275**, 294 (2015).
35. K. J. Kim, M. S. Park, Y. J. Kim, J. H. Kim, S. X. Dou and M. Skyllas-Kazacos, *J. Mater. Chem. A*, **3**, 16913 (2015).
36. Y. K. Zeng, T. S. Zhao, L. An, X. L. Zhou and L. Wei, *J. Power Sources*, **300**, 438 (2015).
37. S. Jung, L. H. Kim, Y. Kwon and S. H. Kim, *Korean J. Chem. Eng.*, **31**, 2081 (2014).
38. X. Luo, Z. Lu, J. Xi, Z. Wu, W. Zhu, L. Chen and X. Qiu, *J. Phys. Chem. B*, **109**, 20310 (2005).
39. M. Jung, W. Lee, N. N. Krishnan, S. Kim, G. Gupta, L. Komsiyska, C. Harms, Y. Kwon and D. Henkensmeier, *Appl. Surf. Sci.*, **450**, 301 (2018).
40. X. L. Zhou, T. S. Zhao, L. An, L. Wei and C. Zhang, *Electrochim. Acta*, **153**, 492 (2015).
41. W. Lee, M. Jung, D. Serhiichuk, G. Gupta, C. Harms, Y. Kwon and D. Henkensmeier, *J. Membr. Sci.*, **591**, 117333 (2019).
42. P. K. Leung, Q. Xu, T. S. Zhao, L. Zeng and C. Zhang, *Electrochim. Acta*, **105**, 584 (2013).
43. Q. Xu, T. S. Zhao and P. K. Leung, *Appl. Energy*, **105**, 47 (2013).
44. W. Li, J. Liu and C. Yan, *Carbon*, **49**, 3463 (2011).
45. S. Wang, X. Zhao, T. Cochell and A. Manthiram, *J. Phys. Chem. Lett.*, **3**, 2164 (2012).
46. Z. Tang, D. S. Aaron, A. B. Papandrew and T. A. Zawodzinski Jr., *ECS Trans.*, **41**, 1 (2012).
47. S. Jeong, S. An, J. Jeong, J. Lee and Y. Kwon, *J. Power Sources*, **278**, 245 (2015).
48. J. Ryu, M. Park and J. Cho, *J. Electrochem. Soc.*, **163**, A5144 (2015).
49. P. T. T. Hien, C. Jo, J. Lee and Y. Kwon, *RSC Adv.*, **6**, 17574 (2016).
50. M. Park, J. Ryu and J. Cho, *Chem. Asian J.*, **10**, 2096 (2015).
51. W. Lee, C. Jo, S. Youk, H. Y. Shin, J. Lee, Y. Chung and Y. Kwon, *Appl. Surf. Sci.*, **429**, 187 (2018).
52. C. Noh, B. W. Kwon, Y. Chung and Y. Kwon, *J. Power Sources*, **438**, 227063 (2019).
53. C. Noh, B. W. Kwon, Y. Chung and Y. Kwon, *J. Power Sources*, **406**, 26 (2018).
54. C. Noh, C. Lee, W. S. Chi, Y. Chung, J. Kim and Y. Kwon, *J. Electrochem. Soc.*, **165**, A1388 (2018).
55. J. Winsberg, T. Hagemann, T. Janoschka, M. D. Hager and U. S. Schubert, *Angew. Chem. Int. Ed.*, **56**, 686 (2017).
56. P. Leung, A. A. Shah, L. Sanz, C. Flox, J. R. Morante, Q. Xu, M. R. Mohamed, C. Ponce de Leon and F. C. Walsh, *J. Power Sources*, **360**, 243 (2017).
57. W. Lee, B. W. Kwon and Y. Kwon, *ACS Appl. Mater. Interfaces*, **10**, 36882 (2018).
58. W. Wang, W. Xu, L. Cosimbescu, D. Choi, L. Li and Z. Yang, *Chem. Commun.*, **48**, 6669 (2012).
59. H. S. Kim, K. J. Lee, Y. K. Han, J. H. Ryu and S. M. Oh, *J. Power Sources*, **348**, 264 (2017).
60. W. Wang and V. Sprenkle, *Nat. Chem.*, **8**, 204 (2016).
61. C. G. Armstrong and K. E. Toghill, *Electrochem. Commun.*, **91**, 19 (2018).
62. M. Shin, C. Noh, Y. Chung and Y. Kwon, *Chem. Eng. J.*, **398**, 125631 (2020).
63. C. Noh, Y. Chung and Y. Kwon, *J. Power Sources*, **466**, 228333 (2020).
64. B. Huskinson, M. P. Marshak, C. Suh, S. Er, M. R. Gerhardt, C. J. Galvin, X. Chen, A. Aspuru-Guzik, R. G. Gordon and M. J. Aziz, *Nature*, **505**, 195 (2014).
65. B. Yang, L. Hoober-Burkhardt, F. Wang, G. S. Prakash and S. R. Narayanan, *J. Electrochem. Soc.*, **161**, A1371 (2014).
66. C. Chu, B. W. Kwon, W. Lee and Y. Kwon, *Korean J. Chem. Eng.*, **36**, 1732 (2019).
67. K. Lin, Q. Chen, M. R. Gerhardt, L. Tong, S. B. Kim, L. Eisenach, A. W. Valle, D. Hardee, R. G. Gordon, M. J. Aziz and M. P. Marshak, *Science*, **349**, 1529 (2015).
68. W. Lee, G. Park and Y. Kwon, *Chem. Eng. J.*, **386**, 123985 (2020).
69. D. G. Kwabi, K. Lin, Y. Ji, E. F. Kerr, M. A. Goulet, D. De Porcellinis, D. P. Tabor, D. A. Pollack, A. Aspuru-Guzik, R. G. Gordon and M. J. Aziz, *Joule*, **2**, 1894 (2018).
70. K. Lin, R. Gómez-Bombarelli, E. S. Beh, L. Tong, Q. Chen, A. Valle, A. Aspuru-Guzik, M. J. Aziz and R. G. Gordon, *Nat. Energy*, **1**, 1 (2016).
71. W. Lee, A. Permatasari, B. W. Kwon and Y. Kwon, *Chem. Eng. J.*, **358**, 1438 (2019).
72. X. Wei, W. Xu, M. Vijayakumar, L. Cosimbescu, T. Liu, V. Sprenkle and W. Wang, *Adv. Mater.*, **26**, 7649 (2014).
73. W. Lee, A. Permatasari and Y. Kwon, *J. Mater. Chem. C*, **8**, 5727 (2020).
74. J. Luo, B. Hu, C. Debruler and T. L. Liu, *Angew. Chem. Int. Ed.*, **57**, 231 (2018).
75. M. Schwaab and J. C. Pinto, *Chem. Eng. Sci.*, **62**, 2750 (2007).
76. G. Renger, G. Christen, M. Karge, H. J. Eckert and K. D. Irrgang, *J. Biol. Inorg. Chem.*, **3**, 360 (1998).
77. K. Hess, H. Morkoc, H. Shichijo and B. G. Streetman, *Appl. Phys. Lett.*, **35**, 469 (1979).
78. X. Wang, J. M. Hu and I. M. Hsing, *J. Electroanal. Chem.*, **562**, 73 (2004).
79. K. Lee and J. D. Nam, *J. Power Sources*, **157**, 201 (2006).
80. J. B. Kingdon and G. J. Ferland, *Astrophys. J. Suppl. Ser.*, **106**, 205 (1996).
81. J. P. Bonvalet and C. de Rouffignac, *J. Physiol.*, **318**, 85 (1981).
82. M. R. Wasielewski, M. P. Niemczyk, W. A. Svec and E. B. Pewitt, *J. Am. Chem. Soc.*, **107**, 1080 (1985).
83. M. N. Tsampas, A. Pikos, S. Brosda, A. Katsaounis and C. G. Vayenas, *Electrochim. Acta*, **51**, 2743 (2006).